A Theory of Fermat Paths for Non-Line-of-Sight Shape Reconstruction: Supplementary Material

Shumian Xin[1], Sotiris Nousias[2,3], Kiriakos N. Kutulakos[2], Aswin C. Sankaranarayanan[1], Srinivasa G. Narasimhan[1], and Ioannis Gkioulekas[1]

[1]Carnegie Mellon University [2]University of Toronto [3]University College London

1. Introduction

In this supplemental material, we cover the following topics:

1. In Section 2, we prove Proposition 2 of the main paper. Additionally, we define the specular and boundary sets for the non-confocal case, and state and prove the analogue of Proposition 2 for this case.
2. In Section 3, we provide more details for the proof of Proposition 3 of the main paper.
3. In Section 4, we prove Proposition 4 of the main paper. Additionally, we state and prove the analogue of Proposition 3 for the non-confocal case.
4. In Section 5, we prove Proposition 5 (Fermat flow equation) of the main paper. Additionally, we state and prove the analogue of Proposition 5 for this case. Moreover, we discuss failure cases of Proposition 5, the curvature information available in higher-order derivatives of the Fermat pathlength function, and how to estimate the gradients used in the Fermat flow equation in the case of a non-planar visible surface $\mathcal{V}$.
5. In Section 6, we discuss our approach for surface fitting under specular pathlength constraints.
6. In Section 7, we discuss details of our reconstruction procedure, and show additional experimental results using synthetic data.

Finally, we include a supplementary video that provides an overview of our theory and reconstruction method, as well as visualizations of some of our measured results.

2. Proposition 2

We prove Proposition 2 of the main paper, which we restate here for convenience.

Proposition 2. *Let $(p,q) \in [0,1]^2$ be a parameterization of the NLOS surface $\mathcal{X}$. Then, for any visible point $\boldsymbol{v}$,*

$$\mathcal{S}(\boldsymbol{v}) = \left\{\boldsymbol{x} \in \mathcal{X} : \nabla_{(p,q)} \tau(\boldsymbol{x}(p,q); \boldsymbol{v}) = \boldsymbol{0}\right\}. \tag{1}$$

Let $r \in [0,1]$ be a parameterization of the NLOS surface boundary $\partial\mathcal{X}$. Then, for any visible point $\boldsymbol{v}$,

$$\mathcal{B}(\boldsymbol{v}) = \left\{\boldsymbol{x} \in \partial\mathcal{X} : \partial\tau(\boldsymbol{x}(r); \boldsymbol{v}) / \partial r = 0\right\}. \tag{2}$$

Proof. For the first part of the proposition, Equation (1), we have,

$$\frac{\partial \tau(\boldsymbol{x}(p,q); \boldsymbol{v})}{\partial p} = \left\langle \frac{\boldsymbol{x}(p,q) - \boldsymbol{v}}{\|\boldsymbol{x}(p,q) - \boldsymbol{v}\|}, \boldsymbol{x}_p(p,q) \right\rangle = \frac{4}{\tau(\boldsymbol{x}(p,q); \boldsymbol{v})} \langle \boldsymbol{x}(p,q) - \boldsymbol{v}, \boldsymbol{x}_p(p,q) \rangle \tag{3}$$

where $\boldsymbol{x}_p(p,q)$ is the partial derivative of $\boldsymbol{x}$ with respect to p. The vector $\boldsymbol{x}_p(p,q)$ is tangent to the surface $\mathcal{X}$ at $\boldsymbol{x}$, and therefore orthogonal to the surface normal $\hat{\boldsymbol{n}}(\boldsymbol{x})$ at that point. If $\boldsymbol{x}(p,q) \in \mathcal{S}(\boldsymbol{v})$, then from the specular reflection property, the vector $\boldsymbol{x}(p,q) - \boldsymbol{v}$ is parallel to the normal $\hat{\boldsymbol{n}}(\boldsymbol{x})$. Therefore,

$$\boldsymbol{x}(p,q) - \boldsymbol{v} \parallel \hat{\boldsymbol{n}}(\boldsymbol{x}) \text{ and } \boldsymbol{x}_p(p,q) \perp \hat{\boldsymbol{n}}(\boldsymbol{x}) \Rightarrow \langle \boldsymbol{x}(p,q) - \boldsymbol{v}, \boldsymbol{x}_p(p,q) \rangle = 0, \tag{4}$$

and from Equation (3),

$$\frac{\partial \tau(\boldsymbol{x}(p,q); \boldsymbol{v})}{\partial p} = 0. \tag{5}$$

The proof for $\frac{\partial \tau(\boldsymbol{x}(p,q);\boldsymbol{v})}{\partial q} = 0$ is exactly the same. Therefore, if $\boldsymbol{x}(p,q) \in \mathcal{S}(\boldsymbol{v})$, then $\nabla_{(p,q)} \tau(\boldsymbol{x}(p,q); \boldsymbol{v}) = \boldsymbol{0}$. Conversely, if $\nabla_{(p,q)} \tau(\boldsymbol{x}(p,q); \boldsymbol{v}) = \boldsymbol{0}$, from Equation (3) we have that either $\boldsymbol{v} = \boldsymbol{x}(p,q)$, or that $\boldsymbol{x}(p,q) - \boldsymbol{v}$ is orthogonal to both $\boldsymbol{x}_p(p,q)$ and $\boldsymbol{x}_q(p,q)$, and therefore parallel to the normal $\hat{\boldsymbol{n}}(\boldsymbol{x})$. By assuming that the visible scene $\mathcal{V}$ and NLOS scene $\mathcal{X}$ are non-intersecting, this implies that $\boldsymbol{x}(p,q) \in \mathcal{S}(\boldsymbol{v})$. This concludes the proof of the first part of the proposition.

For the second part of the proposition, Equation (2), we have,

$$\frac{\partial \tau(\boldsymbol{x}(r); \boldsymbol{v})}{\partial r} = \left\langle \frac{\boldsymbol{x}(r) - \boldsymbol{v}}{\|\boldsymbol{x}(r) - \boldsymbol{v}\|}, \boldsymbol{x}_r(r) \right\rangle = \frac{4}{\tau(\boldsymbol{x}(r); \boldsymbol{v})} \langle \boldsymbol{x}(r) - \boldsymbol{v}, \boldsymbol{x}_r(r) \rangle \tag{6}$$

where $\boldsymbol{x}_r(r)$ is the partial derivative of $\boldsymbol{x}$ with respect to r. The vector $\boldsymbol{x}_r(r)$ is parallel to the tangent $\hat{\boldsymbol{t}}(\boldsymbol{x})$ of the curve $\partial\mathcal{X}$ at $\boldsymbol{x}$. If $\boldsymbol{x}(r) \in \mathcal{B}(\boldsymbol{v})$, then from the property of boundary Fermat paths, the vector $\boldsymbol{x}(r) - \boldsymbol{v}$ is orthogonal to the tangent $\hat{\boldsymbol{t}}(\boldsymbol{x})$. Therefore,

$$\boldsymbol{x}(r) - \boldsymbol{v} \perp \hat{\boldsymbol{t}}(\boldsymbol{x}) \text{ and } \boldsymbol{x}_r(r) \parallel \hat{\boldsymbol{t}}(\boldsymbol{x}) \Rightarrow \langle \boldsymbol{x}(r) - \boldsymbol{v}, \boldsymbol{x}_r(r) \rangle = 0, \tag{7}$$

and from Equation (6),

$$\frac{\partial \tau(\boldsymbol{x}(r); \boldsymbol{v})}{\partial r} = 0. \tag{8}$$

Conversely, if $\frac{\partial \tau(\boldsymbol{x}(r);\boldsymbol{v})}{\partial r} = 0$, from Equation (3) we have that either $\boldsymbol{v} = \boldsymbol{x}(r)$, or that $\boldsymbol{x}(r) - \boldsymbol{v}$ is orthogonal to $\boldsymbol{x}_r(r)$, and therefore orthogonal to $\hat{\boldsymbol{t}}(\boldsymbol{x})$. By assuming that the visible scene $\mathcal{V}$ and the NLOS boundary $\mathcal{BX}$ are non-intersecting, this implies that $\boldsymbol{x}(r) \in \mathcal{B}(\boldsymbol{v})$. This concludes the proof of the second part of the proposition. □

We additionally state Definition 1 and prove the analogue of Proposition 2 of the main paper for the non-confocal case. For this, given two visible points $\boldsymbol{v}_s, \boldsymbol{v}_d \in \mathcal{V}$, and an NLOS point $\boldsymbol{x} \in \mathcal{X}$, we denote by $\boldsymbol{h}(\boldsymbol{x}; \boldsymbol{v}_s, \boldsymbol{v}_d)$ the *half-vector* corresponding to the directions parallel to $\boldsymbol{v}_s - \boldsymbol{x}$ and $\boldsymbol{v}_d - \boldsymbol{x}$.

Definition 2′. *For any two visible points $\boldsymbol{v}_s, \boldsymbol{v}_d \in \mathcal{V}$:*

- *The* specular set $\mathcal{S}(\boldsymbol{v}_s, \boldsymbol{v}_d) \subset \mathcal{X}$ *consists of all points $\boldsymbol{x} \in \mathcal{X} \setminus \partial\mathcal{X}$ such that the half-vector $\boldsymbol{h}(\boldsymbol{x}; \boldsymbol{v}_s, \boldsymbol{v}_d)$ is orthogonal to the tangent plane $T_{\boldsymbol{x}}\mathcal{X}$ of $\mathcal{X}$ at $\boldsymbol{x}$.*
- *The* boundary set $\mathcal{B}(\boldsymbol{v}_s, \boldsymbol{v}_d) \subset \partial\mathcal{X}$ *consists of all points $\boldsymbol{x} \in \nabla\mathcal{X}$ such that the vector $\boldsymbol{h}(\boldsymbol{x}; \boldsymbol{v}_s, \boldsymbol{v}_d)$ is orthogonal to the tangent vector $\hat{\boldsymbol{t}}(\boldsymbol{x})$ of $\partial\mathcal{X}$ at $\boldsymbol{x}$.*
- *The* Fermat set $\mathcal{F}(\boldsymbol{v}_s, \boldsymbol{v}_d) \subset \mathcal{X}$ *is the union of these two sets, $\mathcal{F}(\boldsymbol{v}_s, \boldsymbol{v}_d) \triangleq \mathcal{S}(\boldsymbol{v}_s, \boldsymbol{v}_d) \cup \mathcal{B}(\boldsymbol{v}_s, \boldsymbol{v}_d)$.*

Analogous to the confocal case, for points $\boldsymbol{x} \in \mathcal{S}(\boldsymbol{v}_s, \boldsymbol{v}_d)$, the half-vector $\boldsymbol{h}(\boldsymbol{x}; \boldsymbol{v}_s, \boldsymbol{v}_d)$ is also parallel to the surface normal $\hat{\boldsymbol{n}}(\boldsymbol{x})$. Equivalently, the path $\boldsymbol{p}(\boldsymbol{x}; \boldsymbol{v}_s, \boldsymbol{v}_d) \triangleq \boldsymbol{v}_s \to \boldsymbol{x} \to \boldsymbol{v}_d$ corresponds to a *specular* reflection at $\boldsymbol{x}$. Proposition 2 now becomes as follows.

Proposition 2′. *Let $(p,q) \in [0,1]^2$ be a parameterization of the NLOS surface $\mathcal{X}$. Then, for any pair of visible points $\boldsymbol{v}_s$ and $\boldsymbol{v}_d$,*

$$\mathcal{S}(\boldsymbol{v}_s, \boldsymbol{v}_d) = \left\{ \boldsymbol{x} \in \mathcal{X} : \nabla_{(p,q)} \tau(\boldsymbol{x}(p,q); \boldsymbol{v}_s, \boldsymbol{v}_d) = \boldsymbol{0} \right\}. \tag{9}$$

Let $r \in [0,1]$ be a parameterization of the NLOS surface boundary $\partial\mathcal{X}$. Then, for any pair of visible points $\boldsymbol{v}_s$ and $\boldsymbol{v}_d$,

$$\mathcal{B}(\boldsymbol{v}_s, \boldsymbol{v}_d) = \left\{ \boldsymbol{x} \in \partial\mathcal{X} : \partial\tau(\boldsymbol{x}(r); \boldsymbol{v}_s, \boldsymbol{v}_d) / \partial r = 0 \right\}. \tag{10}$$

Proof. For the first part of the proposition, Equation (9), we have,

$$\frac{\partial \tau\left(\boldsymbol{x}\left(p,q\right);\boldsymbol{v}_s,\boldsymbol{v}_d\right)}{\partial p} = 2\cdot\left\langle \frac{\boldsymbol{x}\left(p,q\right)-\boldsymbol{v}_s}{\left\|\boldsymbol{x}\left(p,q\right)-\boldsymbol{v}_s\right\|}+\frac{\boldsymbol{x}\left(p,q\right)-\boldsymbol{v}_d}{\left\|\boldsymbol{x}\left(p,q\right)-\boldsymbol{v}_d\right\|},\boldsymbol{x}_p\left(p,q\right)\right\rangle = s\left\langle \boldsymbol{h}\left(\boldsymbol{x}\left(p,q\right);\boldsymbol{v}_s,\boldsymbol{v}_d\right),\boldsymbol{x}_p\left(p,q\right)\right\rangle \tag{11}$$

where $\boldsymbol{x}_p\left(p,q\right)$ is the partial derivative of $\boldsymbol{x}$ with respect to p, $\boldsymbol{h}\left(\boldsymbol{x}\left(p,q\right);\boldsymbol{v}_s,\boldsymbol{v}_d\right)$ is the half-vector corresponding to the directions parallel to $\boldsymbol{x}\left(p,q\right)-\boldsymbol{v}_s$ and $\boldsymbol{x}\left(p,q\right)-\boldsymbol{v}_d$, and s some scalar. The vector $\boldsymbol{x}_p\left(p,q\right)$ is tangent to the surface $\mathcal{X}$ at $\boldsymbol{x}$, and therefore orthogonal to the surface normal $\hat{\boldsymbol{n}}\left(\boldsymbol{x}\right)$ at that point. If $\boldsymbol{x}\left(p,q\right)\in\mathcal{S}\left(\boldsymbol{v}_s,\boldsymbol{v}_d\right)$, then from the specular reflection property, the half-vector $\boldsymbol{h}\left(\boldsymbol{x}\left(p,q\right);\boldsymbol{v}_s,\boldsymbol{v}_d\right)$ is parallel to the normal $\hat{\boldsymbol{n}}\left(\boldsymbol{x}\right)$. Therefore,

$$\boldsymbol{h}\left(\boldsymbol{x}\left(p,q\right);\boldsymbol{v}_s,\boldsymbol{v}_d\right)\parallel\hat{\boldsymbol{n}}\left(\boldsymbol{x}\right)\text{ and }\boldsymbol{x}_p\left(p,q\right)\perp\hat{\boldsymbol{n}}\left(\boldsymbol{x}\right)\Rightarrow\left\langle\boldsymbol{h}\left(\boldsymbol{x}\left(p,q\right);\boldsymbol{v}_s,\boldsymbol{v}_d\right),\boldsymbol{x}_p\left(p,q\right)\right\rangle=0, \tag{12}$$

and from Equation (11),

$$\frac{\partial \tau\left(\boldsymbol{x}\left(p,q\right);\boldsymbol{v}_s,\boldsymbol{v}_d\right)}{\partial p}=0. \tag{13}$$

The proof for $\frac{\partial \tau(\boldsymbol{x}(p,q);\boldsymbol{v}_s,\boldsymbol{v}_d)}{\partial q}=0$ is exactly the same. Therefore, if $\boldsymbol{x}\left(p,q\right)\in\mathcal{S}\left(\boldsymbol{v}_s,\boldsymbol{v}_d\right)$, then $\nabla_{(p,q)}\tau\left(\boldsymbol{x}\left(p,q\right);\boldsymbol{v}_s,\boldsymbol{v}_d\right)=\mathbf{0}$. Conversely, if $\nabla_{(p,q)}\tau\left(\boldsymbol{x}\left(p,q\right);\boldsymbol{v}_s,\boldsymbol{v}_d\right)=\mathbf{0}$, from Equation (11) we have that either $\boldsymbol{h}\left(\boldsymbol{x}\left(p,q\right);\boldsymbol{v}_s,\boldsymbol{v}_d\right)=\mathbf{0}$, or that $\boldsymbol{h}\left(\boldsymbol{x}\left(p,q\right);\boldsymbol{v}_s,\boldsymbol{v}_d\right)$ is orthogonal to both $\boldsymbol{x}_p\left(p,q\right)$ and $\boldsymbol{x}_q\left(p,q\right)$, and therefore parallel to the normal $\hat{\boldsymbol{n}}\left(\boldsymbol{x}\right)$. By assuming that the visible points $\boldsymbol{v}_s$ and $\boldsymbol{v}_d$ must be on the same side of the NLOS scene $\mathcal{X}$, this implies that $\boldsymbol{x}\left(p,q\right)\in\mathcal{S}\left(\boldsymbol{v}_s,\boldsymbol{v}_d\right)$. This concludes the proof of the first part of the proposition.

For the second part of the proposition, Equation (10), we have,

$$\frac{\partial \tau\left(\boldsymbol{x}\left(r\right);\boldsymbol{v}_s,\boldsymbol{v}_d\right)}{\partial r} = 2\cdot\left\langle \frac{\boldsymbol{x}\left(r\right)-\boldsymbol{v}_s}{\left\|\boldsymbol{x}\left(r\right)-\boldsymbol{v}_s\right\|}+\frac{\boldsymbol{x}\left(r\right)-\boldsymbol{v}_d}{\left\|\boldsymbol{x}\left(r\right)-\boldsymbol{v}_d\right\|},\boldsymbol{x}_p\left(r\right)\right\rangle = s\left\langle \boldsymbol{h}\left(\boldsymbol{x}\left(r\right);\boldsymbol{v}_s,\boldsymbol{v}_d\right),\boldsymbol{x}_p\left(r\right)\right\rangle \tag{14}$$

where $\boldsymbol{x}_r\left(r\right)$ is the partial derivative of $\boldsymbol{x}$ with respect to r. The vector $\boldsymbol{x}_r\left(r\right)$ is parallel to the tangent $\hat{\boldsymbol{t}}\left(\boldsymbol{x}\right)$ of the curve $\partial\mathcal{X}$ at $\boldsymbol{x}$. If $\boldsymbol{x}\left(r\right)\in\mathcal{B}\left(\boldsymbol{v}\right)$, then from the property of boundary Fermat paths, the half-vector $\boldsymbol{h}\left(\boldsymbol{x}\left(r\right);\boldsymbol{v}_s,\boldsymbol{v}_d\right)$ is orthogonal to the tangent $\hat{\boldsymbol{t}}\left(\boldsymbol{x}\right)$. Therefore,

$$\boldsymbol{h}\left(\boldsymbol{x}\left(r\right),\boldsymbol{v}_s,\boldsymbol{v}_d\right)\perp\hat{\boldsymbol{t}}\left(\boldsymbol{x}\right)\text{ and }\boldsymbol{x}_r\left(r\right)\parallel\hat{\boldsymbol{t}}\left(\boldsymbol{x}\right)\Rightarrow\left\langle\boldsymbol{h}\left(\boldsymbol{x}\left(p,q\right);\boldsymbol{v}_s,\boldsymbol{v}_d\right),\boldsymbol{x}_r\left(r\right)\right\rangle=0, \tag{15}$$

and from Equation (14),

$$\frac{\partial \tau\left(\boldsymbol{x}\left(r\right);\boldsymbol{v}_s,\boldsymbol{v}_d\right)}{\partial r}=0. \tag{16}$$

Conversely, if $\frac{\partial \tau(\boldsymbol{x}(r);\boldsymbol{v}_s,\boldsymbol{v}_d)}{\partial r}=0$, from Equation (11) we have that either $\boldsymbol{h}\left(\boldsymbol{x}\left(p,q\right);\boldsymbol{v}_s,\boldsymbol{v}_d\right)=\mathbf{0}$, or that $\boldsymbol{h}\left(\boldsymbol{x}\left(p,q\right);\boldsymbol{v}_s,\boldsymbol{v}_d\right)$ is orthogonal to $\boldsymbol{x}_r\left(r\right)$, and therefore orthogonal to $\hat{\boldsymbol{t}}\left(\boldsymbol{x}\right)$. By assuming that the visible points $\boldsymbol{v}_s$ and $\boldsymbol{v}_d$ are at the same side of the boundary $\mathcal{BX}$, this implies that $\boldsymbol{x}\left(r\right)\in\mathcal{B}\left(\boldsymbol{v}_s,\boldsymbol{v}_d\right)$. This concludes the proof of the second part of the proposition. □

3. Proposition 3

We provide more details for the proof of Proposition 3 of the main paper, which we restate here for convenience.

Proposition 3. *Assume that the BRDF of the $\mathcal{X}$ surface is non-zero in the specular direction. Then, for all $\boldsymbol{x}\in\mathcal{F}\left(\boldsymbol{v}\right)$, the transient $I\left(\tau;\boldsymbol{v}\right)$ will have a discontinuity at pathlength $\tau\left(\boldsymbol{x};\boldsymbol{v}\right)$. If $\boldsymbol{x}\in\mathcal{S}\left(\boldsymbol{v}\right)$, then $I\left(\tau;\boldsymbol{v}\right)$ will additionally have a vertical asymptote at $\tau\left(\boldsymbol{x};\boldsymbol{v}\right)$.*

Proof. Let $\mathrm{Sph}\left(\rho;\boldsymbol{v}\right)$ be the sphere of center $\boldsymbol{v}$ and radius ρ. Let $\mathcal{C}\left(\rho;\boldsymbol{v}\right)$ be the intersection of $\mathrm{Sph}\left(\rho;\boldsymbol{v}\right)$ with $\mathcal{X}$, parameterized by $c\in[0,1]$. Then, we can use $(c,\rho)\in[0,1]\times[0,\infty)$ to reparameterize $\mathcal{X}$. We note, however, that this parameterization is continuously-differentiable only *locally*, separating the surface $\mathcal{X}$ into submanifolds $\mathcal{M}_i$ within which this condition holds. These submanifolds are separated by occluding contours or surface boundaries (including surface discontinuities). We can then express the transient $I\left(\tau;\boldsymbol{v}\right)$ as

$$I\left(\tau;\boldsymbol{v}\right)=\sum_{\mathcal{M}_i}\int_{\mathcal{M}_i} f\left(\boldsymbol{x};\boldsymbol{v}\right)\delta\left(\tau-\tau\left(\boldsymbol{x};\boldsymbol{v}\right)\right)\left|\mathcal{J}^{(c,\rho)}_{(p,q)}\left(\boldsymbol{x}\right)\right|^{-1}\mathrm{d}A\left(c,\rho\right), \tag{17}$$

where (p, q) is the parameterization of $\mathcal{X}$ $\mathcal{J}^{(c,\rho)}_{(p,q)}(\boldsymbol{x})$ is the Jacobian of the transformation $(p, q) \mapsto (c, \rho)$. We also consider the transient produced by each submanifold,

$$I_{\mathcal{M}_i}(\tau; \boldsymbol{v}) = \int_{\mathcal{M}_i} f(\boldsymbol{x}; \boldsymbol{v}) \, \delta(\tau - \tau(\boldsymbol{x}; \boldsymbol{v})) \left| \mathcal{J}^{(c,\rho)}_{(p,q)}(\boldsymbol{x}) \right|^{-1} \tag{18}$$

$$udA(c, \rho), \tag{19}$$

Within each submanifold, the parameter ρ has a range $\rho \in [\rho_{\text{min}}, \rho_{\text{max}}]$. Recognizing that at each point $\boldsymbol{x} \in \mathcal{M}_i$, $\rho(\boldsymbol{x}) = \tau(\boldsymbol{x}; \boldsymbol{v})/2$, and from the definition of the boundary and specular sets, the extrema of ρ will occur either at points on an occluding contour (in which case the corresponding value of $I_{\mathcal{M}_i}$ will be zero), at boundary points $\boldsymbol{x} \in \mathcal{B}(\boldsymbol{v})$, or at specular points $\boldsymbol{x} \in \mathcal{S}(\boldsymbol{v})$. In the boundary case, the corresponding transient $I_{\mathcal{M}_i}$ will be discontinuous at $\tau = 2\rho$:

- If ρ is a maximum, then $I_{\mathcal{M}_i} > 0$ as $\tau \to 2\rho^-$, and $I_{\mathcal{M}_i} = 0$ as $\tau \to 2\rho^+$.
- If ρ is a minimum, then $I_{\mathcal{M}_i} > 0$ as $\tau \to 2\rho^+$, and $I_{\mathcal{M}_i} = 0$ as $\tau \to 2\rho^-$.

Consequently, the transient I will also have a discontinuity at the same point.

We now consider the particular case of a point $\boldsymbol{x}_{\mathcal{S}} \in \mathcal{S}(\boldsymbol{v})$. Recognizing that $\rho(\boldsymbol{x}_{\mathcal{S}}) = \tau(\boldsymbol{x}_{\mathcal{S}}; \boldsymbol{v})/2$, we have from Equation (1) that $\nabla_{(p,q)} \rho(\boldsymbol{x}_{\mathcal{S}}) = \mathbf{0}$. Consequently,

$$abs\mathcal{J}^{(c,\rho)}_{(p,q)}(\boldsymbol{x}_{\mathcal{S}}) = \frac{\partial \rho(\boldsymbol{x}_{\mathcal{S}})}{\partial p} \frac{\partial c(\boldsymbol{x}_{\mathcal{S}})}{\partial q} - \frac{\partial \rho(\boldsymbol{x}_{\mathcal{S}})}{\partial q} \frac{\partial c(\boldsymbol{x}_{\mathcal{S}})}{\partial p} = 0. \tag{20}$$

Then, from Equations (19) and (17), at $\tau = \tau(\boldsymbol{x}_{\mathcal{S}}; \boldsymbol{v})$, the corresponding transient $I_{\mathcal{M}_i}$ and the total transient I converge to infinity, resulting in a discontinuity. As in the boundary case, we can distinguish whether I converges to infinity as $\tau \to 2\rho(\boldsymbol{x}_{\mathcal{S}})^-$ or $\tau \to 2\rho(\boldsymbol{x}_{\mathcal{S}})^+$ depending on whether $\tau(\boldsymbol{x}_{\mathcal{S}}; \boldsymbol{v})$ is a minimum or maximum, respectively. □

We note that the discussion in Section 2.2. of the main paper about identifying the type of stationarity of a discontinuity follows directly from the above proof of Proposition 3.

We additionally state and prove the analogue of Proposition 3 of the main paper for the non-confocal case.

Proposition 3′. *Assume that the BRDF of the $\mathcal{X}$ surface is non-zero in the specular direction. Then, for all $\boldsymbol{x} \in \mathcal{F}(\boldsymbol{v}_s, \boldsymbol{v}_d)$, the transient $I(\tau; \boldsymbol{v}_s, \boldsymbol{v}_d)$ will have a discontinuity at pathlength $\tau(\boldsymbol{x}; \boldsymbol{v}_s, \boldsymbol{v}_d)$. If $\boldsymbol{x} \in \mathcal{S}(\boldsymbol{v}_s, \boldsymbol{v}_d)$, then $I(\tau; \boldsymbol{v}_s, \boldsymbol{v}_d)$ will additionally have a local maximum at $\tau(\boldsymbol{x}; \boldsymbol{v}_s, \boldsymbol{v}_d)$.*

Proof. Let $E(\tau; \boldsymbol{v}_s, \boldsymbol{v}_d)$ be the ellipsoid of foci $\boldsymbol{v}_s$ and $\boldsymbol{v}_d$, and pathlength τ. Let $\mathcal{C}(\tau; \boldsymbol{v}_s, \boldsymbol{v}_d)$ be the intersection of $E(\tau; \boldsymbol{v}_s, \boldsymbol{v}_d)$ with $\mathcal{X}$, parameterized by $c \in [0, 1]$. Then, we can use $(c, \tau) \in [0, 1] \times [0, \infty)$ to reparameterize $\mathcal{X}$. The rest of the proof follows exactly analogously to the proof of Proposition 3 for the confocal case. □

4. Proposition 4

We prove Proposition 4 of the main paper, which we restate here for convenience.

Proposition 4. *Let a transient $I(\tau; \boldsymbol{v})$ have a* specular *discontinuity at $\tau_{\mathcal{S}}$, corresponding to a point $\boldsymbol{x}_{\mathcal{S}} \in \mathcal{S}(\boldsymbol{v})$. If $\kappa_{min}, \kappa_{max}$ are the principal curvatures of $\mathcal{X}$ at $\boldsymbol{x}_{\mathcal{S}}$, then:*

- *If $\tau_{\mathcal{S}}$ is a local minimum of $\tau(\boldsymbol{x}; \boldsymbol{v})$, $2/\tau_{\mathcal{S}} < \kappa_{min}$.*
- *If $\tau_{\mathcal{S}}$ is a local maximum of $\tau(\boldsymbol{x}; \boldsymbol{v})$, $\kappa_{max} < 2/\tau_{\mathcal{S}}$.*
- *If $\tau_{\mathcal{S}}$ is a saddle point of $\tau(\boldsymbol{x}; \boldsymbol{v})$, $\kappa_{min} \leq 2/\tau_{\mathcal{S}} \leq \kappa_{max}$.*

Proof. As $\tau_{\mathcal{S}}$ is a discontinuity corresponding to a specular path, the sphere $\text{Sph}(\rho_{\mathcal{S}}; \boldsymbol{v})$ of radius $\rho_{\mathcal{S}} = \tau_{\mathcal{S}}/2$ and center $\boldsymbol{v}$ will be tangent to the NLOS surface at point $\boldsymbol{x}_{\mathcal{S}}$.

We consider first the case where $\tau_{\mathcal{S}}$ is a local minimum of $\tau(\boldsymbol{x}; \boldsymbol{v})$. Then, there will be some neighborhood $\mathcal{N}(\boldsymbol{x}_{\mathcal{S}}) \subset \mathcal{X}$ of $\boldsymbol{x}_{\mathcal{S}}$ on $\mathcal{X}$ such that, for all points $\boldsymbol{x} \in \mathcal{N}(\boldsymbol{x}_{\mathcal{S}})$, $\tau(\boldsymbol{x}; \boldsymbol{v}) \geq \tau_{\mathcal{S}}$. Equivalently, all of $\mathcal{N}(\boldsymbol{x}_{\mathcal{S}})$ lies outside the sphere $\text{Sph}(\rho_{\mathcal{S}}; \boldsymbol{v})$, and is tangent to that sphere at the point $\boldsymbol{x}_{\mathcal{S}}$. Therefore, the curves on $\mathcal{N}(\boldsymbol{x}_{\mathcal{S}})$ passing through $\boldsymbol{x}_{\mathcal{S}}$ in all possible tangent directions are also tangent to and outside of the sphere $\text{Sph}(\rho_{\mathcal{S}}; \boldsymbol{v})$. Consequently, all normal curvatures of

$\mathcal{X}$ at $\boldsymbol{x}_{\mathcal{S}}$ are greater than the inverse of the radius of $\mathrm{Sph}\left(\rho_{\mathcal{S}};\boldsymbol{v}\right)$. From the definition of principal curvatures, we conclude that $2/\tau_{\mathcal{S}}=\rho_{\mathcal{S}}\leq\kappa_{\min}$.

The case when $\tau_{\mathcal{S}}$ is a local maximum of $\tau\left(\boldsymbol{x};\boldsymbol{v}\right)$ proceeds very similarly: In this case, all of $\mathcal{N}\left(\boldsymbol{x}_{\mathcal{S}}\right)$ is *inside* the sphere $\mathrm{Sph}\left(\rho_{\mathcal{S}};\boldsymbol{v}\right)$, and tangent to it at $\boldsymbol{x}_{\mathcal{S}}$. Therefore, the curves on $\mathcal{N}\left(\boldsymbol{x}_{\mathcal{S}}\right)$ passing through $\boldsymbol{x}_{\mathcal{S}}$ in all possible tangent directions are also tangent to and *inside* of the sphere $\mathrm{Sph}\left(\rho_{\mathcal{S}};\boldsymbol{v}\right)$. Consequently, all normal curvatures of $\mathcal{X}$ at $\boldsymbol{x}_{\mathcal{S}}$ are *smaller* than the inverse of the radius of $\mathrm{Sph}\left(\rho_{\mathcal{S}};\boldsymbol{v}\right)$. From the definition of principal curvatures, we conclude that $\kappa_{\max}\leq\rho_{\mathcal{S}}=2/\tau_{\mathcal{S}}$.

Finally, we proceed similarly for the case $\tau_{\mathcal{S}}$ is a saddle point of $\tau\left(\boldsymbol{x};\boldsymbol{v}\right)$: In this case, $\mathcal{N}\left(\boldsymbol{x}_{\mathcal{S}}\right)$ lies partially inside and partially outside the sphere $\mathrm{Sph}\left(\rho_{\mathcal{S}};\boldsymbol{v}\right)$. Therefore, while all the curves on $\mathcal{N}\left(\boldsymbol{x}_{\mathcal{S}}\right)$ passing through $\boldsymbol{x}_{\mathcal{S}}$ in all possible tangent directions are still tangent to the sphere $\mathrm{Sph}\left(\rho_{\mathcal{S}};\boldsymbol{v}\right)$; some of them will be inside and some outside of the $\mathrm{Sph}\left(\rho_{\mathcal{S}};\boldsymbol{v}\right)$. Consequently, there exist normal curvatures of $\mathcal{X}$ at $\boldsymbol{x}_{\mathcal{S}}$ that are smaller, and others that are greater than the inverse of the radius of $\mathrm{Sph}\left(\rho_{\mathcal{S}};\boldsymbol{v}\right)$. From the definition of principal curvatures, we conclude that $\kappa_{\min}\leq\rho_{\mathcal{S}}=2/\tau_{\mathcal{S}}\leq\kappa_{\max}$. □

We additionally state and prove the analogue of Proposition 4 of the main paper for the non-confocal case.

Proposition 4′. *Let a transient $I\left(\tau;\boldsymbol{v}_s,\boldsymbol{v}_d\right)$ have a* specular *discontinuity at $\tau_{\mathcal{S}}$, corresponding to a point $\boldsymbol{x}_{\mathcal{S}}\in\mathcal{S}\left(\boldsymbol{v}_s,\boldsymbol{v}_d\right)$. Let $E\left(\tau_{\mathcal{S}};\boldsymbol{v}_s,\boldsymbol{v}_d\right)$ be the corresponding osculating ellipsoid. If $\kappa_{min},\kappa_{max}$ are the principal curvatures of $\mathcal{X}$ at $\boldsymbol{x}_{\mathcal{S}}$, and $\lambda_{min},\lambda_{max}$ the principal curvatures of $E\left(\tau_{\mathcal{S}};\boldsymbol{v}_s,\boldsymbol{v}_d\right)$ at $\boldsymbol{x}_{\mathcal{S}}$, then:*

- *If $\tau_{\mathcal{S}}$ is a local minimum of $\tau\left(\boldsymbol{x};\boldsymbol{v}_d,\boldsymbol{v}_s\right)$, then $\lambda_{min}\leq\kappa_{min}$.*
- *If $\tau_{\mathcal{S}}$ is a local maximum of $\tau\left(\boldsymbol{x};\boldsymbol{v}_d,\boldsymbol{v}_s\right)$, then $\kappa_{max}\leq\lambda_{max}$.*

Proof. We consider first the case where $\tau_{\mathcal{S}}$ is a local minimum of $\tau\left(\boldsymbol{x};\boldsymbol{v}_s,\boldsymbol{v}_d\right)$. Then, there will be some neighborhood $\mathcal{N}\left(\boldsymbol{x}_{\mathcal{S}}\right)\subset\mathcal{X}$ of $\boldsymbol{x}_{\mathcal{S}}$ on $\mathcal{X}$ such that, for all points $\boldsymbol{x}\in\mathcal{N}\left(\boldsymbol{x}_{\mathcal{S}}\right)$, $\tau\left(\boldsymbol{x};\boldsymbol{v}_s,\boldsymbol{v}_d\right)\geq\tau_{\mathcal{S}}$. Equivalently, all of $\mathcal{N}\left(\boldsymbol{x}_{\mathcal{S}}\right)$ lies outside the ellipsoid $E\left(\tau_{\mathcal{S}};\boldsymbol{v}_s,\boldsymbol{v}_d\right)$, and is tangent to that ellipsoid at the point $\boldsymbol{x}_{\mathcal{S}}$. Therefore, the curves on $\mathcal{N}\left(\boldsymbol{x}_{\mathcal{S}}\right)$ passing through $\boldsymbol{x}_{\mathcal{S}}$ in all possible tangent directions are also tangent to and outside of the ellipsoid $E\left(\tau_{\mathcal{S}};\boldsymbol{v}_s,\boldsymbol{v}_d\right)$. Consequently, all normal curvatures of $\mathcal{X}$ at $\boldsymbol{x}_{\mathcal{S}}$ are greater than the smallest normal curvature of the ellipsoid $E\left(\tau_{\mathcal{S}};\boldsymbol{v}_s,\boldsymbol{v}_d\right)$ at $\boldsymbol{x}_{\mathcal{S}}$. From the definition of principal curvatures, we conclude that $\lambda_{\min}\leq\kappa_{\min}$.

The case when $\tau_{\mathcal{S}}$ is a local maximum of $\tau\left(\boldsymbol{x};\boldsymbol{v}_s,\boldsymbol{v}_d\right)$ proceeds very similarly: In this case, all of $\mathcal{N}\left(\boldsymbol{x}_{\mathcal{S}}\right)$ is *inside* the ellipsoid $E\left(\tau_{\mathcal{S}};\boldsymbol{v}_s,\boldsymbol{v}_d\right)$, and tangent to it at $\boldsymbol{x}_{\mathcal{S}}$. Therefore, the curves on $\mathcal{N}\left(\boldsymbol{x}_{\mathcal{S}}\right)$ passing through $\boldsymbol{x}_{\mathcal{S}}$ in all possible tangent directions are also tangent to and *inside* of the ellipsoid $E\left(\tau_{\mathcal{S}};\boldsymbol{v}_s,\boldsymbol{v}_d\right)$. Consequently, all normal curvatures of $\mathcal{X}$ at $\boldsymbol{x}_{\mathcal{S}}$ are *smaller* than the largest normal curvature of the ellipsoid $E\left(\tau_{\mathcal{S}};\boldsymbol{v}_s,\boldsymbol{v}_d\right)$ at $\boldsymbol{x}_{\mathcal{S}}$. From the definition of principal curvatures, we conclude that $\kappa_{\max}\leq\lambda_{\max}$.

□

5. Proposition 5—Fermat flow equation

We prove Proposition 5 of the main paper (the Fermat flow equation), which we restate here for convenience.

Proposition 5. *Consider a branch of the Fermat pathlength function $\tau_{\mathcal{F}}\left(\boldsymbol{v}\right)$ evaluated at $\boldsymbol{v}\in\mathcal{V}$. Assume that there is a unique point $\boldsymbol{x}_{\mathcal{F}}\in\mathcal{F}\left(\boldsymbol{v}\right)$ with $\tau\left(\boldsymbol{x}_{\mathcal{F}};\boldsymbol{v}\right)=\tau_{\mathcal{F}}\left(\boldsymbol{v}\right)$. Then,*

$$\nabla_{\boldsymbol{v}}\tau_{\mathcal{F}}\left(\boldsymbol{v}\right)=-2\frac{\boldsymbol{x}_{\mathcal{F}}-\boldsymbol{v}}{\left\|\boldsymbol{x}_{\mathcal{F}}-\boldsymbol{v}\right\|}. \tag{21}$$

Proof. We will be using $\boldsymbol{v}=\left[v^x,v^y,v^z\right]^T$ to denote the 3D coordinates of the point $\boldsymbol{v}$, and similarly for all other vectors.

We first prove the proposition for the case of a *specular* discontinuity, that is, $\boldsymbol{x}_{\mathcal{F}}\in\mathcal{S}\left(\boldsymbol{v}\right)$. Let $(p,q)\in[0,1]^2$ be a parameterization of the NLOS surface $\mathcal{X}$ in a neighborhood around $\boldsymbol{x}_{\mathcal{F}}$, such that $\boldsymbol{x}_{\mathcal{F}}=\boldsymbol{x}\left(p\left(\boldsymbol{v}\right),q\left(\boldsymbol{v}\right)\right)$. We consider each

coordinate of the vector $\nabla_{\boldsymbol{v}}\tau_{\mathcal{F}}(\boldsymbol{v})$ separately. For the first coordinate, we have

$$\frac{\partial\tau_{\mathcal{F}}(\boldsymbol{v})}{\partial v^x} = 2\frac{\partial\left\|\boldsymbol{x}_{\mathcal{F}}-\boldsymbol{v}\right\|}{\partial v^x} \tag{22}$$

$$= 2\frac{\partial\left\|\boldsymbol{x}\left(p(\boldsymbol{v}),q(\boldsymbol{v})\right)-\boldsymbol{v}\right\|}{\partial v^x} \tag{23}$$

$$= 2\left\langle\frac{\boldsymbol{x}\left(p(\boldsymbol{v}),q(\boldsymbol{v})\right)-\boldsymbol{v}}{\left\|\boldsymbol{x}\left(p(\boldsymbol{v}),q(\boldsymbol{v})\right)-\boldsymbol{v}\right\|},\frac{\partial\left(\boldsymbol{x}\left(p(\boldsymbol{v}),q(\boldsymbol{v})\right)-\boldsymbol{v}\right)}{\partial v^x}\right\rangle \tag{24}$$

$$= 2\left\langle\frac{\boldsymbol{x}_{\mathcal{F}}-\boldsymbol{v}}{\left\|\boldsymbol{x}_{\mathcal{F}}-\boldsymbol{v}\right\|},\boldsymbol{x}_p\left(p(\boldsymbol{v}),q(\boldsymbol{v})\right)\frac{\partial p(\boldsymbol{v})}{\partial v^x}+\boldsymbol{x}_q\left(p(\boldsymbol{v}),q(\boldsymbol{v})\right)\frac{\partial q(\boldsymbol{v})}{\partial v^x}-[1,0,0]^T\right\rangle \tag{25}$$

$$= \frac{2}{\left\|\boldsymbol{x}_{\mathcal{F}}-\boldsymbol{v}\right\|}\left(\left\langle\boldsymbol{x}_{\mathcal{F}}-\boldsymbol{v},\boldsymbol{x}_p\left(p(\boldsymbol{v}),q(\boldsymbol{v})\right)\right\rangle\frac{\partial p(\boldsymbol{v})}{\partial v^x}+\left\langle\boldsymbol{x}_{\mathcal{F}}-\boldsymbol{v},\boldsymbol{x}_q\left(p(\boldsymbol{v}),q(\boldsymbol{v})\right)\right\rangle\frac{\partial q(\boldsymbol{v})}{\partial v^x}-\left\langle\boldsymbol{x}_{\mathcal{F}}-\boldsymbol{v},[1,0,0]^T\right\rangle\right). \tag{26}$$

In Equation (26), the vectors $\boldsymbol{x}_p\left(p(\boldsymbol{v}),q(\boldsymbol{v})\right)$ and $\boldsymbol{x}_q\left(p(\boldsymbol{v}),q(\boldsymbol{v})\right)$ are tangent to the NLOS surface $\mathcal{X}$ at $\boldsymbol{x}_{\mathcal{F}}$. Given that we assumed that $\boldsymbol{x}_{\mathcal{F}}\in\mathcal{S}\boldsymbol{v}$, and from the definition of the specular set, the vector $\boldsymbol{x}_{\mathcal{F}}-\boldsymbol{v}$ is parallel to the normal $\hat{\boldsymbol{n}}(\boldsymbol{x}_{\mathcal{F}})$ of $\mathcal{X}$ at $\boldsymbol{x}_{\mathcal{F}}$. Therefore, $\boldsymbol{x}_{\mathcal{F}}-\boldsymbol{v}$ is orthogonal to $\boldsymbol{x}_p\left(p(\boldsymbol{v}),q(\boldsymbol{v})\right)$ and $\boldsymbol{x}_q\left(p(\boldsymbol{v}),q(\boldsymbol{v})\right)$, and Equation (26) becomes

$$\frac{\partial\tau_{\mathcal{F}}(\boldsymbol{v})}{\partial v^x} = \frac{2}{\left\|\boldsymbol{x}_{\mathcal{F}}-\boldsymbol{v}\right\|}\left(0\cdot\frac{\partial p(\boldsymbol{v})}{\partial v^x}+0\cdot\frac{\partial q(\boldsymbol{v})}{\partial v^x}-\left\langle\boldsymbol{x}_{\mathcal{F}}-\boldsymbol{v},[1,0,0]^T\right\rangle\right)=-2\frac{\left(\boldsymbol{x}_{\mathcal{F}}-\boldsymbol{v}\right)^x}{\left\|\boldsymbol{x}_{\mathcal{F}}-\boldsymbol{v}\right\|}. \tag{27}$$

Exactly analogously, we can prove that

$$\frac{\partial\tau_{\mathcal{F}}(\boldsymbol{v})}{\partial v^y}=-2\frac{\left(\boldsymbol{x}_{\mathcal{F}}-\boldsymbol{v}\right)^y}{\left\|\boldsymbol{x}_{\mathcal{F}}-\boldsymbol{v}\right\|} \qquad \text{and} \qquad \frac{\partial\tau_{\mathcal{F}}(\boldsymbol{v})}{\partial v^z}=-2\frac{\left(\boldsymbol{x}_{\mathcal{F}}-\boldsymbol{v}\right)^z}{\left\|\boldsymbol{x}_{\mathcal{F}}-\boldsymbol{v}\right\|}. \tag{28}$$

Combining Equations (27) and (28) completes the proof for the specular case.

We now prove the proposition for the case of a *boundary* discontinuity, that is, $\boldsymbol{x}_{\mathcal{F}}\in\mathcal{B}(\boldsymbol{v})$. Let $r\in[0,1]$ be a parameterization of the NLOS surface boundary $\partial\mathcal{X}$ in a neighborhood around $\boldsymbol{x}_{\mathcal{F}}$, such that $\boldsymbol{x}_{\mathcal{F}}=\boldsymbol{x}(r(\boldsymbol{v}))$. We again consider each coordinate of the vector $\nabla_{\boldsymbol{v}}\tau_{\mathcal{F}}(\boldsymbol{v})$ separately. For the first coordinate, we have

$$\frac{\partial\tau_{\mathcal{F}}(\boldsymbol{v})}{\partial v^x} = 2\frac{\partial\left\|\boldsymbol{x}_{\mathcal{F}}-\boldsymbol{v}\right\|}{\partial v^x} \tag{29}$$

$$= 2\frac{\partial\left\|\boldsymbol{x}\left(r(\boldsymbol{v})\right)-\boldsymbol{v}\right\|}{\partial v^x} \tag{30}$$

$$= 2\left\langle\frac{\boldsymbol{x}\left(r(\boldsymbol{v})\right)-\boldsymbol{v}}{\left\|\boldsymbol{x}\left(r(\boldsymbol{v})\right)-\boldsymbol{v}\right\|},\frac{\partial\left(\boldsymbol{x}\left(r(\boldsymbol{v})\right)-\boldsymbol{v}\right)}{\partial v^x}\right\rangle \tag{31}$$

$$= 2\left\langle\frac{\boldsymbol{x}_{\mathcal{F}}-\boldsymbol{v}}{\left\|\boldsymbol{x}_{\mathcal{F}}-\boldsymbol{v}\right\|},\boldsymbol{x}_r\left(r(\boldsymbol{v})\right)\frac{\partial r(\boldsymbol{v})}{\partial v^x}-[1,0,0]^T\right\rangle \tag{32}$$

$$= \frac{2}{\left\|\boldsymbol{x}_{\mathcal{F}}-\boldsymbol{v}\right\|}\left(\left\langle\boldsymbol{x}_{\mathcal{F}}-\boldsymbol{v},\boldsymbol{x}_r\left(r(\boldsymbol{v})\right)\right\rangle\frac{\partial r(\boldsymbol{v})}{\partial v^x}-\left\langle\boldsymbol{x}_{\mathcal{F}}-\boldsymbol{v},[1,0,0]^T\right\rangle\right). \tag{33}$$

In Equation (33), the vector $\boldsymbol{x}_r\left(r(\boldsymbol{v})\right)$ is parallel to the tangent $\hat{\boldsymbol{t}}(\boldsymbol{x}_{\mathcal{F}})$ of the NLOS surface boundary $\partial\mathcal{X}$ at $\boldsymbol{x}_{\mathcal{F}}$. Given that we assumed that $\boldsymbol{x}_{\mathcal{F}}\in\mathcal{B}(\boldsymbol{v})$, and from the definition of the boundary set, the vector $\boldsymbol{x}_{\mathcal{F}}-\boldsymbol{v}$ is orthogonal to the tangent $\hat{\boldsymbol{t}}(\boldsymbol{x}_{\mathcal{F}})$. Therefore, $\boldsymbol{x}_{\mathcal{F}}-\boldsymbol{v}$ is also orthogonal to $\boldsymbol{x}_r\left(r(\boldsymbol{v})\right)$, and Equation (33) becomes

$$\frac{\partial\tau_{\mathcal{F}}(\boldsymbol{v})}{\partial v^x} = \frac{2}{\left\|\boldsymbol{x}_{\mathcal{F}}-\boldsymbol{v}\right\|}\left(0\cdot\frac{\partial r(\boldsymbol{v})}{\partial v^x}-\left\langle\boldsymbol{x}_{\mathcal{F}}-\boldsymbol{v},[1,0,0]^T\right\rangle\right)=-2\frac{\left(\boldsymbol{x}_{\mathcal{F}}-\boldsymbol{v}\right)^x}{\left\|\boldsymbol{x}_{\mathcal{F}}-\boldsymbol{v}\right\|}. \tag{34}$$

Exactly analogously, we can prove that

$$\frac{\partial\tau_{\mathcal{F}}(\boldsymbol{v})}{\partial v^y}=-2\frac{\left(\boldsymbol{x}_{\mathcal{F}}-\boldsymbol{v}\right)^y}{\left\|\boldsymbol{x}_{\mathcal{F}}-\boldsymbol{v}\right\|} \qquad \text{and} \qquad \frac{\partial\tau_{\mathcal{F}}(\boldsymbol{v})}{\partial v^z}=-2\frac{\left(\boldsymbol{x}_{\mathcal{F}}-\boldsymbol{v}\right)^z}{\left\|\boldsymbol{x}_{\mathcal{F}}-\boldsymbol{v}\right\|}. \tag{35}$$

Combining Equations (34) and (35) completes the proof for the boundary case. □

We additionally state and prove the analogue of Proposition 5 of the main paper for the non-confocal case. convenience.

Proposition 5′. *Consider a branch of the Fermat pathlength function $\tau_{\mathcal{F}}(\boldsymbol{v}_s, \boldsymbol{v}_d)$ corresponding to visible points $\boldsymbol{v}_s, \boldsymbol{v}_d \in \mathcal{V}$. Assume that there is a unique point $\boldsymbol{x}_{\mathcal{F}} \in \mathcal{F}(\boldsymbol{v}_s, \boldsymbol{v}_d)$ with $\tau(\boldsymbol{x}_{\mathcal{F}}; \boldsymbol{v}_s, \boldsymbol{v}_d) = \tau_{\mathcal{F}}(\boldsymbol{v}_s, \boldsymbol{v}_d)$. Then,*

$$\nabla_{\boldsymbol{v}_s} \tau_{\mathcal{F}}(\boldsymbol{v}_s, \boldsymbol{v}_d) = -\frac{\boldsymbol{x}_{\mathcal{F}} - \boldsymbol{v}_s}{\|\boldsymbol{x}_{\mathcal{F}} - \boldsymbol{v}_s\|} \qquad \textit{and} \qquad \nabla_{\boldsymbol{v}_d} \tau_{\mathcal{F}}(\boldsymbol{v}_s, \boldsymbol{v}_d) = -\frac{\boldsymbol{x}_{\mathcal{F}} - \boldsymbol{v}_d}{\|\boldsymbol{x}_{\mathcal{F}} - \boldsymbol{v}_d\|}. \tag{36}$$

Proof. We will prove Equation (36) only for $\nabla_{\boldsymbol{v}_s} \tau_{\mathcal{F}}(\boldsymbol{v}_s, \boldsymbol{v}_d)$, as the proof for $\nabla_{\boldsymbol{v}_d} \tau_{\mathcal{F}}(\boldsymbol{v}_s, \boldsymbol{v}_d)$ is exactly analogous. We will be using $\boldsymbol{v}_s = [v_s^x, v_s^y, v_s^z]^T$ to denote the 3D coordinates of the point $\boldsymbol{v}_s$, and similarly for all other vectors.

We first prove the proposition for the case of a *specular* discontinuity, that is, $\boldsymbol{x}_{\mathcal{F}} \in \mathcal{S}(\boldsymbol{v}_s, \boldsymbol{v}_d)$. Let $(p, q) \in [0, 1]^2$ be a parameterization of the NLOS surface $\mathcal{X}$ in a neighborhood $\mathcal{N} \subset \mathcal{X}$ around $\boldsymbol{x}_{\mathcal{F}}$, such that $\boldsymbol{x}_{\mathcal{F}} = \boldsymbol{x}(p(\boldsymbol{v}_s, \boldsymbol{v}_d), q(\boldsymbol{v}_s, \boldsymbol{v}_d))$.

We use $\mathcal{O}$ to denote the *orthotomic* surface corresponding to $\mathcal{N}$ with respect to the point $\boldsymbol{v}_d$ [5, 4]. For each pair of points $\boldsymbol{v}_s$ and $\boldsymbol{x}_{\mathcal{F}} \in \mathcal{S}(\boldsymbol{v}_s, \boldsymbol{v}_d)$, the orthotomic contains a corresponding point $\boldsymbol{o}_{\mathcal{F}} = \boldsymbol{o}(p(\boldsymbol{v}_s, \boldsymbol{v}_d), q(\boldsymbol{v}_s, \boldsymbol{v}_d))$ such that

$$\|\boldsymbol{o}_{\mathcal{F}} - \boldsymbol{v}_s\| = \tau_{\mathcal{F}}, \qquad \text{and} \qquad \hat{\boldsymbol{n}}(\boldsymbol{o}_{\mathcal{F}}) = -\frac{\boldsymbol{x}_{\mathcal{F}} - \boldsymbol{v}_s}{\|\boldsymbol{x}_{\mathcal{F}} - \boldsymbol{v}_s\|} = -\frac{\boldsymbol{o}_{\mathcal{F}} - \boldsymbol{v}_s}{\|\boldsymbol{o}_{\mathcal{F}} - \boldsymbol{v}_s\|}, \tag{37}$$

where $\hat{\boldsymbol{n}}(\boldsymbol{o}_{\mathcal{F}})$ is the normal of the orthotomic $\mathcal{O}$ at $\boldsymbol{o}_{\mathcal{F}}$. Additionally, the parameterization (p, q) can be used to parameterize the orthotomic as well, through the mapping from points of the neighborhood $\mathcal{N}$ to $\mathcal{O}$. For more about the properties of the orthotomic, we refer to [5, 4].

We now consider each coordinate of the vector $\nabla_{\boldsymbol{v}_s} \tau_{\mathcal{F}}(\boldsymbol{v}_s, \boldsymbol{v}_d)$ separately. For the first coordinate, and using Equation (37), we have

$$\frac{\partial \tau_{\mathcal{F}}(\boldsymbol{v}_s, \boldsymbol{v}_d)}{\partial v_s^x} = \frac{\partial \|\boldsymbol{o}_{\mathcal{F}} - \boldsymbol{v}_s\|}{\partial v_s^x} \tag{38}$$

$$= \frac{\partial \|\boldsymbol{o}(p(\boldsymbol{v}_s, \boldsymbol{v}_d), q(\boldsymbol{v}_s, \boldsymbol{v}_d)) - \boldsymbol{v}_s\|}{\partial v^x} \tag{39}$$

$$= \left\langle \frac{\boldsymbol{o}(p(\boldsymbol{v}_s, \boldsymbol{v}_d), q(\boldsymbol{v}_s, \boldsymbol{v}_d)) - \boldsymbol{v}_s}{\|\boldsymbol{o}(p(\boldsymbol{v}_s, \boldsymbol{v}_d), q(\boldsymbol{v}_s, \boldsymbol{v}_d)) - \boldsymbol{v}_s\|}, \frac{\partial (\boldsymbol{o}(p(\boldsymbol{v}_s, \boldsymbol{v}_d), q(\boldsymbol{v}_s, \boldsymbol{v}_d)) - \boldsymbol{v}_s)}{\partial v_s^x} \right\rangle \tag{40}$$

$$= \left\langle \frac{\boldsymbol{o}_{\mathcal{F}} - \boldsymbol{v}_s}{\|\boldsymbol{o}_{\mathcal{F}} - \boldsymbol{v}_s\|}, \boldsymbol{o}_p(p(\boldsymbol{v}_s, \boldsymbol{v}_d), q(\boldsymbol{v}_s, \boldsymbol{v}_d)) \frac{\partial p(\boldsymbol{v}_s, \boldsymbol{v}_d)}{\partial v_s^x} + \boldsymbol{o}_q(p(\boldsymbol{v}_s, \boldsymbol{v}_d), q(\boldsymbol{v}_s, \boldsymbol{v}_d)) \frac{\partial q(\boldsymbol{v}_s, \boldsymbol{v}_d)}{\partial v_s^x} - [1, 0, 0]^T \right\rangle. \tag{41}$$

In Equation (41), we can use Equation (37) to replace $\hat{\boldsymbol{n}}(\boldsymbol{o}_{\mathcal{F}})$, which gives us

$$\begin{aligned} \frac{\partial \tau_{\mathcal{F}}(\boldsymbol{v}_s, \boldsymbol{v}_d)}{\partial v_s^x} = &- \langle \hat{\boldsymbol{n}}(\boldsymbol{o}_{\mathcal{F}}), \boldsymbol{o}_p(p(\boldsymbol{v}_s, \boldsymbol{v}_d), q(\boldsymbol{v}_s, \boldsymbol{v}_d)) \rangle \frac{\partial p(\boldsymbol{v}_s, \boldsymbol{v}_d)}{\partial v_s^x} \\ &- \langle \hat{\boldsymbol{n}}(\boldsymbol{o}_{\mathcal{F}}), \boldsymbol{o}_q(p(\boldsymbol{v}_s, \boldsymbol{v}_d), q(\boldsymbol{v}_s, \boldsymbol{v}_d)) \rangle \frac{\partial q(\boldsymbol{v}_s, \boldsymbol{v}_d)}{\partial v_s^x} \\ &- \left\langle \hat{\boldsymbol{n}}(\boldsymbol{o}_{\mathcal{F}}), [1, 0, 0]^T \right\rangle. \end{aligned} \tag{42}$$

In Equation (42), the vectors $\boldsymbol{o}_p(p(\boldsymbol{v}_s, \boldsymbol{v}_d), q(\boldsymbol{v}_s, \boldsymbol{v}_d))$ and $\boldsymbol{o}_q(p(\boldsymbol{v}_s, \boldsymbol{v}_d), q(\boldsymbol{v}_s, \boldsymbol{v}_d))$ are tangent to the orthotomic surface $\mathcal{O}$ at $\boldsymbol{o}_{\mathcal{F}}$, and therefore orthogonal to the normal $\hat{\boldsymbol{n}}(\boldsymbol{o}_{\mathcal{F}})$ at that point. Consequently, and using Equation (37), Equation (42) becomes

$$\frac{\partial \tau_{\mathcal{F}}(\boldsymbol{v}_s, \boldsymbol{v}_d)}{\partial v_s^x} = -0 \cdot \frac{\partial p(\boldsymbol{v}_s, \boldsymbol{v}_d)}{\partial v_s^x} - 0 \cdot \frac{\partial q(\boldsymbol{v}_s, \boldsymbol{v}_d)}{\partial v_s^x} - (\hat{\boldsymbol{n}}(\boldsymbol{o}_{\mathcal{F}}))^x = -\frac{(\boldsymbol{x}_{\mathcal{F}} - \boldsymbol{v}_s)^x}{\|\boldsymbol{x}_{\mathcal{F}} - \boldsymbol{v}_s\|}. \tag{43}$$

Exactly analogously, we can prove that

$$\frac{\partial \tau_{\mathcal{F}}(\boldsymbol{v}_s, \boldsymbol{v}_d)}{\partial v_s^y} = -\frac{(\boldsymbol{x}_{\mathcal{F}} - \boldsymbol{v}_s)^y}{\|\boldsymbol{x}_{\mathcal{F}} - \boldsymbol{v}_s\|} \qquad \text{and} \qquad \frac{\partial \tau_{\mathcal{F}}(\boldsymbol{v}_s, \boldsymbol{v}_d)}{\partial v_s^z} = -\frac{(\boldsymbol{x}_{\mathcal{F}} - \boldsymbol{v}_s)^z}{\|\boldsymbol{x}_{\mathcal{F}} - \boldsymbol{v}_s\|}. \tag{44}$$

Combining Equations (43) and (44) completes the proof for the specular case.

We now prove the proposition for the case of a *boundary* discontinuity, that is, $\boldsymbol{x}_{\mathcal{F}} \in \mathcal{B}(\boldsymbol{v}_s, \boldsymbol{v}_d)$. Let $r \in [0,1]$ be a parameterization of the NLOS surface boundary $\partial\mathcal{X}$ in a neighborhood $\mathcal{M} \subset \mathcal{B}\mathcal{X}$ around $\boldsymbol{x}_{\mathcal{F}}$, such that $\boldsymbol{x}_{\mathcal{F}} = \boldsymbol{x}(r(\boldsymbol{v}_s, \boldsymbol{v}_d))$.

As in the specular case, we consider the orthotomic curve $\mathcal{Q}$ of $\mathcal{M}$ with respect to the point $\boldsymbol{v}_d$ [5, 4]. For each pair of points $\boldsymbol{v}_s$ and $\boldsymbol{x}_{\mathcal{F}} \in \mathcal{B}(\boldsymbol{v}_s, \boldsymbol{v}_d)$, the orthotomic contains a corresponding point $\boldsymbol{q}_{\mathcal{F}} = \boldsymbol{q}(r(\boldsymbol{v}_s, \boldsymbol{v}_d))$ such that

$$\|\boldsymbol{q}_{\mathcal{F}} - \boldsymbol{v}_s\| = \tau_{\mathcal{F}}, \qquad \text{and} \qquad \hat{\boldsymbol{t}}(\boldsymbol{q}_{\mathcal{F}}) \perp -\frac{\boldsymbol{x}_{\mathcal{F}} - \boldsymbol{v}_s}{\|\boldsymbol{x}_{\mathcal{F}} - \boldsymbol{v}_s\|} = -\frac{\boldsymbol{q}_{\mathcal{F}} - \boldsymbol{v}_s}{\|\boldsymbol{q}_{\mathcal{F}} - \boldsymbol{v}_s\|}, \tag{45}$$

where $\hat{\boldsymbol{t}}(\boldsymbol{q}_{\mathcal{F}})$ is the tangent to the orthotomic $\mathcal{Q}$ at $\boldsymbol{q}_{\mathcal{F}}$. Additionally, the parameterization r can be used to parameterize the orthotomic curve as well, through the mapping from points of the neighborhood $\mathcal{M}$ to $\mathcal{Q}$.

We now consider each coordinate of the vector $\nabla_{\boldsymbol{v}_s}\tau_{\mathcal{F}}(\boldsymbol{v}_s, \boldsymbol{v}_d)$ separately. For the first coordinate, and using Equation (45), we have

$$\begin{aligned}
\frac{\partial\tau_{\mathcal{F}}(\boldsymbol{v}_s, \boldsymbol{v}_d)}{\partial v_s^x} &= \frac{\partial\|\boldsymbol{q}_{\mathcal{F}} - \boldsymbol{v}_s\|}{\partial v_s^x} && (46)\\
&= \frac{\partial\|\boldsymbol{q}(r(\boldsymbol{v}_s, \boldsymbol{v}_d)) - \boldsymbol{v}_s\|}{\partial v^x} && (47)\\
&= \left\langle \frac{\boldsymbol{q}(r(\boldsymbol{v}_s, \boldsymbol{v}_d)) - \boldsymbol{v}_s}{\|\boldsymbol{q}(r(\boldsymbol{v}_s, \boldsymbol{v}_d)) - \boldsymbol{v}_s\|}, \frac{\partial(\boldsymbol{q}(r(\boldsymbol{v}_s, \boldsymbol{v}_d)) - \boldsymbol{v}_s)}{\partial v_s^x} \right\rangle && (48)\\
&= \left\langle \frac{\boldsymbol{q}_{\mathcal{F}} - \boldsymbol{v}_s}{\|\boldsymbol{q}_{\mathcal{F}} - \boldsymbol{v}_s\|}, \boldsymbol{q}_r(r(\boldsymbol{v}_s, \boldsymbol{v}_d)) \frac{\partial r(\boldsymbol{v}_s, \boldsymbol{v}_d)}{\partial v_s^x} - [1,0,0]^T \right\rangle && (49)\\
&= \left\langle \frac{\boldsymbol{q}_{\mathcal{F}} - \boldsymbol{v}_s}{\|\boldsymbol{q}_{\mathcal{F}} - \boldsymbol{v}_s\|}, \boldsymbol{q}_r(r(\boldsymbol{v}_s, \boldsymbol{v}_d)) \right\rangle \frac{\partial r(\boldsymbol{v}_s, \boldsymbol{v}_d)}{\partial v_s^x} - \left\langle \frac{\boldsymbol{q}_{\mathcal{F}} - \boldsymbol{v}_s}{\|\boldsymbol{q}_{\mathcal{F}} - \boldsymbol{v}_s\|}, [1,0,0]^T \right\rangle. && (50)
\end{aligned}$$

In Equation (50), the vector $\boldsymbol{q}_r(r(\boldsymbol{v}_s, \boldsymbol{v}_d))$ is parallel to the tanget $\hat{\boldsymbol{t}}(\boldsymbol{q}_{\mathcal{F}})$ of the orthotomic $\mathcal{Q}$ at $\boldsymbol{q}_{\mathcal{F}}$. Therefore, using Equation (45), we can write

$$\frac{\partial\tau_{\mathcal{F}}(\boldsymbol{v}_s, \boldsymbol{v}_d)}{\partial v_s^x} = 0\frac{\partial r(\boldsymbol{v}_s, \boldsymbol{v}_d)}{\partial v_s^x} - \left\langle \frac{\boldsymbol{q}_{\mathcal{F}} - \boldsymbol{v}_s}{\|\boldsymbol{q}_{\mathcal{F}} - \boldsymbol{v}_s\|}, [1,0,0]^T \right\rangle = -\frac{(\boldsymbol{x}_{\mathcal{F}} - \boldsymbol{v}_s)^x}{\|\boldsymbol{x}_{\mathcal{F}} - \boldsymbol{v}_s\|} \tag{51}$$

Exactly analogously, we can prove that

$$\frac{\partial\tau_{\mathcal{F}}(\boldsymbol{v}_s, \boldsymbol{v}_d)}{\partial v_s^y} = -\frac{(\boldsymbol{x}_{\mathcal{F}} - \boldsymbol{v}_s)^y}{\|\boldsymbol{x}_{\mathcal{F}} - \boldsymbol{v}_s\|} \qquad \text{and} \qquad \frac{\partial\tau_{\mathcal{F}}(\boldsymbol{v}_s, \boldsymbol{v}_d)}{\partial v_s^z} = -\frac{(\boldsymbol{x}_{\mathcal{F}} - \boldsymbol{v}_s)^z}{\|\boldsymbol{x}_{\mathcal{F}} - \boldsymbol{v}_s\|}. \tag{52}$$

Combining Equations (51) and (52) completes the proof for the boundary case. □

We note that, in the proof of Proposition 5′, we effectively use the orthotomic to convert the problem into an equivalent problem for a confocal case.

5.1. Discussion of the Fermat flow equation

We discuss various aspects of the Fermat flow equation. We focus on the confocal case (Proposition 5), but most of the discussion applies exactly analogously to the non-confocal case (Proposition 5′).

Non-existence of gradient. Proposition 5 requires that the point $\boldsymbol{x}_{\mathcal{F}}$ be unique for each pathlength $\tau_{\mathcal{F}}$ where a transient discontinuity occurs. This requirement can be violated when there are more than one points in $\mathcal{F}(\boldsymbol{v}) \subset \mathcal{X}$ that are equidistant from $\boldsymbol{v}$. For an extreme example of this, we can consider an NLOS surface $\mathcal{X}$ that is a hemisphere, resulting from cutting a sphere along a plane. Then, this uniqueness requirement will be violated for all points $\boldsymbol{v}$ on the line that passes through the center of the hemisphere and is orthogonal to the cutting plane. In particular, when $\boldsymbol{v}$ is the center of the hemisphere, then its Fermat set is the entire hemisphere, $\mathcal{F}(\boldsymbol{v}) = \mathcal{X}$, and all points in this set are equidistant from $\boldsymbol{v}$. When $\boldsymbol{v}$ is some other point on the line, then its boundary set is the entire boundary of the hemisphere, $\mathcal{B}(\boldsymbol{v}) = \partial\mathcal{X}$, and all points in this set are equidistant from $\boldsymbol{v}$. For more general NLOS surfaces $\mathcal{X}$, the uniqueness condition can be violated for points satisfying various symmetries, and in particular, points on the *skeleton* (or medial axis) of the surface.

When the uniqueness condition of Proposition 5 is violated, then the gradient of Equation (21) does not exist. As we will see below, this can result in isolated spurious point reconstructions.

Second-order derivatives. Proposition 5 motivates the question: Can we extract any additional information about the NLOS surface $\mathcal{X}$ from, say, second-order derivatives of $\tau_{\mathcal{F}}(\boldsymbol{v})$? In the case of *specular* paths, the answer is affirmative: Considering that the first-order derivatives of $\tau_{\mathcal{F}}(\boldsymbol{v})$ correspond to the direction of specular reflection, the second-order derivatives correspond to the *moving specularity* an observer placed at $\boldsymbol{v}$ would notice if the NLOS surface $\mathcal{X}$ were specular. Then, it is known from classical papers on specular geometry that this movement can be related to the local curvature of the NLOS surface $\mathcal{X}$ at the point of reflection $\boldsymbol{x}_{\mathcal{F}}$ [13]. When considering the global minimum branch of $\tau_{\mathcal{F}}(\boldsymbol{v})$, then the Laplacian of $\tau_{\mathcal{F}}(\boldsymbol{v})$ is equivalent to the Laplacian of the distance function, which can likewise be related to the (mean) curvature of the surface $\mathcal{X}$ [10].

Gradient estimation on general visible surfaces. Unfortunately, we cannot directly measure the gradient $\nabla_{\boldsymbol{v}}\tau_{\mathcal{F}}(\boldsymbol{v})$ used in Proposition 5. Moreover, in NLOS imaging settings, we do not have the freedom to vary $\boldsymbol{v}$ in three dimensions. Instead, $\boldsymbol{v}$ is constrained to lie on a visible surface $\mathcal{V}$. As we show below, we can still estimate the gradient from perturbations of $\boldsymbol{v}$ on any general surface $\mathcal{V}$.

For this, we assume that $\mathcal{V}$ can be parameterized by $(m,n)\in[0,1]^2$, and therefore $\boldsymbol{v}=[v^x(m,n),v^y(m,n),v^z(m,n)]^T$. If $\boldsymbol{x}_{\mathcal{F}}$ is specular, $\boldsymbol{x}_{\mathcal{F}}\in\mathcal{S}(\boldsymbol{v})$ then, by performing a calculation similar to the one in Equations (22)-(27), we have

$$\frac{\partial\tau_{\mathcal{F}}(\boldsymbol{v})}{\partial m}=2\frac{\partial\left\|\boldsymbol{x}_{\mathcal{F}}-\boldsymbol{v}\right\|}{\partial m} \tag{53}$$

$$=2\frac{\partial\left\|\boldsymbol{x}\left(p(\boldsymbol{v}),q(\boldsymbol{v})\right)-\boldsymbol{v}\right\|}{\partial m} \tag{54}$$

$$=2\left\langle\frac{\boldsymbol{x}\left(p(\boldsymbol{v}),q(\boldsymbol{v})\right)-\boldsymbol{v}}{\left\|\boldsymbol{x}\left(p(\boldsymbol{v}),q(\boldsymbol{v})\right)-\boldsymbol{v}\right\|},\frac{\partial\left(\boldsymbol{x}\left(p(\boldsymbol{v}),q(\boldsymbol{v})\right)-\boldsymbol{v}\right)}{\partial m}\right\rangle \tag{55}$$

$$=2\left\langle\frac{\boldsymbol{x}_{\mathcal{F}}-\boldsymbol{v}}{\left\|\boldsymbol{x}_{\mathcal{F}}-\boldsymbol{v}\right\|},\boldsymbol{x}_p\left(p(\boldsymbol{v}),q(\boldsymbol{v})\right)\frac{\partial p(\boldsymbol{v})}{\partial m}+\boldsymbol{x}_q\left(p(\boldsymbol{v}),q(\boldsymbol{v})\right)\frac{\partial q(\boldsymbol{v})}{\partial v^x}-\boldsymbol{v}_m\right\rangle \tag{56}$$

$$=\frac{2}{\left\|\boldsymbol{x}_{\mathcal{F}}-\boldsymbol{v}\right\|}\left(\left\langle\boldsymbol{x}_{\mathcal{F}}-\boldsymbol{v},\boldsymbol{x}_p\left(p(\boldsymbol{v}),q(\boldsymbol{v})\right)\right\rangle\frac{\partial p(\boldsymbol{v})}{\partial m}+\left\langle\boldsymbol{x}_{\mathcal{F}}-\boldsymbol{v},\boldsymbol{x}_q\left(p(\boldsymbol{v}),q(\boldsymbol{v})\right)\right\rangle\frac{\partial q(\boldsymbol{v})}{\partial m}-\left\langle\boldsymbol{x}_{\mathcal{F}}-\boldsymbol{v},\boldsymbol{v}_m\right\rangle\right). \tag{57}$$

where $\boldsymbol{v}_m=\left[\frac{\partial v^x(m,n)}{\partial m},\frac{\partial v^y(m,n)}{\partial m},\frac{\partial v^z(m,n)}{\partial m}\right]^T$ is tangent to the surface $\mathcal{V}$ at $\boldsymbol{v}$. Using the fact that the vectors $\boldsymbol{x}_p\left(p(\boldsymbol{v}),q(\boldsymbol{v})\right)$ and $\boldsymbol{x}_q\left(p(\boldsymbol{v}),q(\boldsymbol{v})\right)$ are tangent to the NLOS surface $\mathcal{X}$ at $\boldsymbol{x}_{\mathcal{F}}$, and therefore orthogonal to $\boldsymbol{x}_{\mathcal{F}}-\boldsymbol{v}$, Equation (57) becomes

$$\frac{\partial\tau_{\mathcal{F}}(\boldsymbol{v})}{\partial m}=-2\left\langle\frac{\boldsymbol{x}_{\mathcal{F}}-\boldsymbol{v}}{\left\|\boldsymbol{x}_{\mathcal{F}}-\boldsymbol{v}\right\|},\boldsymbol{v}_m\right\rangle. \tag{58}$$

Exactly analogously, we have,

$$\frac{\partial\tau_{\mathcal{F}}(\boldsymbol{v})}{\partial n}=-2\left\langle\frac{\boldsymbol{x}_{\mathcal{F}}-\boldsymbol{v}}{\left\|\boldsymbol{x}_{\mathcal{F}}-\boldsymbol{v}\right\|},\boldsymbol{v}_n\right\rangle. \tag{59}$$

We can also prove Equations (58)-(59) for the boundary case, $\boldsymbol{x}_{\mathcal{F}}\in\mathcal{B}(\boldsymbol{v})$, by likewise adapting the calculation of Equations (29)-(34).

We can select the parameterization (m,n) such that the tangent vectors $\boldsymbol{v}_m,\boldsymbol{v}_n$ are of unit norm and orthogonal to each other (e.g., by making the tangent vectors be the principal curvature directions). Then Equations (58) and (59) correspond simply to rotating coordinate system axes, from the global coordinate system to the local coordinate system at $\boldsymbol{v}$ with axes $\boldsymbol{v}_m,\boldsymbol{v}_n,\boldsymbol{v}_m\times\boldsymbol{v}_n$. In this coordinate system, the gradient will equal:

$$\left(\frac{\partial\tau_{\mathcal{F}}(\boldsymbol{v})}{\partial m},\frac{\partial\tau_{\mathcal{F}}(\boldsymbol{v})}{\partial n},\sqrt{4-\left(\frac{\partial\tau_{\mathcal{F}}(\boldsymbol{v})}{\partial m}\right)^2-\left(\frac{\partial\tau_{\mathcal{F}}(\boldsymbol{v})}{\partial n}\right)^2}\right), \tag{60}$$

where the first two terms can be estimated by perturbing the point $\boldsymbol{v}$ on the visible surface $\mathcal{V}$ and interpolating. Finally, by performing a rotation, we can obtain from Equation (60) the gradient $\nabla_{\boldsymbol{v}}\tau_{\mathcal{F}}(\boldsymbol{v})$ in the global coordinate system. For a planar surface $\mathcal{V}$, the above discussion reduces to Equation (11) of the main paper.

We note that Equation (60), as well as Equation (11) of the main paper, assume that the gradient $\nabla_{\boldsymbol{v}}\tau_{\mathcal{F}}(\boldsymbol{v})$ exists. When the uniqueness condition of Proposition 5 is not satisfied, these equations are invalid and will result in spurious reconstructed points.

6. Surface fitting under specular pathlength constraints

We provide details about the surface fitting procedure discussed in Section 3 of the main paper. The fact that our reconstruction relies on interpolated estimates, rather than direct measurements, of $\nabla_{\boldsymbol{v}}\tau_{\mathcal{F}}(\boldsymbol{v})$ can potentially introduce some error in the reconstructed point cloud and fitted surface. We can improve the accuracy of an initial surface reconstruction by modifying it so that it more closely matches the set $\{\tau_{\mathcal{F}}(\boldsymbol{v}_m), m = 1, \ldots, M\}$ of Fermat pathlength measurements available to us. This requires solving an optimization problem of the form:

$$\min_{\mathcal{S}} \sum_{m=1}^{M} \left\| \tau_{\mathcal{F}}(\boldsymbol{v}_m) - \tau_{\mathcal{F}}(\mathcal{S}, \boldsymbol{v}_m) \right\|^2, \tag{61}$$

where for a surface $\mathcal{S}$ and a point $\boldsymbol{v}$, the function $\tau_{\mathcal{F}}(\mathcal{S}, \boldsymbol{v})$ returns the length of the Fermat path between $\boldsymbol{v}$ and points on $\mathcal{S}$. This is a challenging *geometric* optimization problem, because of the difficulty of evaluating $\tau_{\mathcal{F}}(\mathcal{S}, \boldsymbol{v})$, and because the function $\tau_{\mathcal{F}}(\mathcal{S}, \boldsymbol{v})$ can be multi-valued.

To simplify exposition, we consider the case where we perform fitting for a single Fermat pathlength measurement $\tau_{\mathcal{F}}(\boldsymbol{v})$. We also assume that the surface $\mathcal{S}$ is a triangular mesh of fixed topology, consisting of K triangles, $\mathcal{S} = \bigcup_{k=1}^{K} \mathcal{T}_k$, and V vertices. For each triangle $\mathcal{T}_k$, the 3×3 matrix $\boldsymbol{V}_k$ contains the 3D coordinates of the triangle's three vertices. We use $\boldsymbol{V}$ to denote the $3 \times V$ matrix containing the 3D coordinates of all mesh vertices.

Then, Equation (61) is simplified to:

$$\min_{\boldsymbol{V}} \left\| \tau_{\mathcal{F}}(\boldsymbol{v}) - \tau_{\mathcal{F}}(\mathcal{S}, \boldsymbol{v}) \right\|^2, \tag{62}$$

To *approximately* solve the optimization problem of Equation (62), we begin by identifying specular points on the current mesh $\mathcal{S}$ with respect to $\boldsymbol{v}$. This involves solving the specular *forward projection* problem [1, 2, 3]):

$$\min_{\mathcal{T}_k, k=1,\ldots,K} \min_{\boldsymbol{x} \in \mathcal{T}_k} \left\| 1 - \left\langle \frac{\boldsymbol{v} - \boldsymbol{x}}{\|\boldsymbol{v} - \boldsymbol{x}\|}, \hat{\boldsymbol{n}}(\boldsymbol{x}) \right\rangle \right\|^2. \tag{63}$$

Within each triangle $\mathcal{T}_k$, the inner optimization problem of Equation (63) can be solved by parameterizing points on the triangle using barycentric coordinates and then using gradient descent on this parametric representation. To accelerate both the inner and outer optimization problems, we use the sub-triangle search and triangle-prunning techniques from Walter et al. [12]. We denote by $\mathcal{T}^*$ the triangle containing the point $\boldsymbol{x} \in \mathcal{S}$ where the minimum of Equation (63) occurs. When Equation (63) has multiple solutions (multiple points on $\boldsymbol{x} \in \mathcal{S}$ forming specular paths with respect to $\boldsymbol{v}$), we select among these solutions the point that minimizes the difference $\|\tau_{\mathcal{F}}(\boldsymbol{v}) - \tau(\boldsymbol{x}; \boldsymbol{v})\|$; that is, the point that most closely matches the available Fermat pathlength measurement.

We then approximate the problem of Equation (62) with the simpler problem

$$\min_{\boldsymbol{V}^*} \left\| \tau_{\mathcal{F}}(\boldsymbol{v}) - \tau(\boldsymbol{x}^*, \boldsymbol{v}) \right\|^2, \tag{64}$$

where

$$\boldsymbol{x}^* = \operatorname*{argmin}_{\boldsymbol{x} \in \mathcal{T}^*} \left\| 1 - \left\langle \frac{\boldsymbol{v} - \boldsymbol{x}}{\|\boldsymbol{v} - \boldsymbol{x}\|}, \hat{\boldsymbol{n}}(\boldsymbol{x}) \right\rangle \right\|^2, \tag{65}$$

and $\boldsymbol{V}^*$ are the vertices of triangle $\mathcal{T}^*$. The difficulty in solving the optimization problem of Equation (64) comes from the fact that the point $\boldsymbol{x}^*$ is defined *implicitly* as a function of the vertices $\boldsymbol{V}^*$, through the second optimization problem of Equation (65). Nonetheless, we can use the *implicit function theorem* [11] to compute the derivative of $\boldsymbol{x}^*$ with respect to the vertex coordinates $\boldsymbol{V}^*$. This derivative is given by Jakob and Marschner [8], and in our case, we use automatic differentiation to compute the corresponding Jacobian terms. Given this, we can optimize Equation (64) using gradient descent.

In using the above procedure, we have made a number of assumptions:

- We assume that the available Fermat pathlength measurement $\tau_{\mathcal{F}}(\boldsymbol{v})$ is a *specular* pathlength, when it can also be a boundary pathlength. In practice, we use the following heuristic to remove measurements that are likely to be boundary pathlengths: We discard any measurements for which the forward projection problem of Equation (63) does not have a good solution (loss function below some threshold).

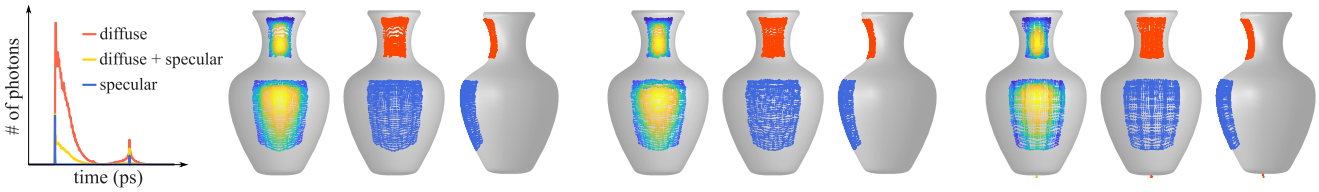

(a) simulated transients (b) reconstruction for diffuse case (c) reconstruction for diffuse+specular case (d) reconstruction for specular case

Figure 1: **Reconstructions under different BRDFs.** We show reconstructions from simulated transient measurements for a vase, rendered under three different BRDFs: Lambertian, mixture of Lambertian and specular, and specular. (a) Comparison of rendered transients for the three cases (representative sample). (b)-(d) For each case, we show reconstructed points colored by normal (left) and by branch of the Fermat pathlength function (middle and right).

- We identify the measurement $\tau_{\mathcal{F}}(\boldsymbol{v})$ with the point $\boldsymbol{x} \in \mathcal{S}$, among the solutions of the forward projection problem, whose pathlength $\tau(\boldsymbol{x}; \boldsymbol{v})$ is the closest to the measurement. It is possible that $\tau_{\mathcal{F}}(\boldsymbol{v})$ may correspond to a different specular point. In practice, we found this heuristic to work well.
- When approximating Equation (62) with Equation (64), we do not take into account that, as the surface deforms, the triangle $\mathcal{T}^*$ that contains the point $\boldsymbol{x}$ producing the specular path may change. In practice, we address this by alternating between the optimization problems of Equations (64) and (63).

Finally, we mention that when we have more than one Fermat pathlength measurements $\{\tau_{\mathcal{F}}(\boldsymbol{v}_m), m = 1, \ldots, M\}$, the same vertex in $\boldsymbol{V}$ can be used by more than one triangles $\mathcal{T}_m^*$, each corresponding to the solution of the forward projection for measurement $\tau_{\mathcal{F}}(\boldsymbol{v}_m)$. In that case, during optimization, each vertex is updated by the sum of the gradients for all problems (64) affecting it.

7. Simulated experiments

In this section, we use synthetic data to evaluate the performance of our reconstruction algorithm under different BRDF and noise conditions. In all cases, the synthetic data was simulated using physically-accurate Monte Carlo rendering [7], and noise was added using the SPAD model of Hernandez et al. [6].

Algorithmic details. We discuss some details of our reconstruction pipeline. In particular, our reconstruction algorithm requires identifying points of discontinuity in each measured transient $I(\tau, \boldsymbol{v})$. We do this with a basic one-dimensional edge detection procedure, by filtering each transient with a set of derivative-of-Gaussian filters, and performing non-max-suppression. To compute gradients $\nabla_{\boldsymbol{v}} \tau_{\mathcal{F}}(\boldsymbol{v})$, we use quadratic interpolation on Fermat pathlength values at a 5×5 neighborhood around each point $\boldsymbol{v}$. After reconstructing an oriented point cloud using the Fermat flow algorithm, we fit a surface to it using Poisson surface reconstruction [9], then optimize this surface using the method of Section 6.

Reconstructions under different BRDFs and noise levels. Figures 1 and 2 show simulated experiments for a vase object. We render 64×64 transients under a confocal scanning scheme. The Fermat pathlength function for the vase object has two branches, both specular, one corresponding to the convex body of the vase, and another to the concave neck of the vase.

In Figure 1, we compare rendered data and reconstructions for three different BRDFs, ranging from fully Lambertian to fully specular. We observe that both the reconstructed normals and points remain largely invariant to the BRDF change, as expected from our theory.

In Figure 2, we compare rendered data and reconstructions for three different noise levels. We observe again that the reconstructions of both normals and points remain robust as the noise increases.

References

[1] Amit Agrawal, Yuichi Taguchi, and Srikumar Ramalingam. Analytical forward projection for axial non-central dioptric and catadioptric cameras. In *European Conference on Computer Vision*, pages 129–143. Springer, 2010. 10

[2] Amit Agrawal, Yuichi Taguchi, and Srikumar Ramalingam. Beyond alhazen's problem: Analytical projection model for non-central catadioptric cameras with quadric mirrors. In *Computer Vision and Pattern Recognition (CVPR), 2011 IEEE Conference on*, pages 2993–3000. IEEE, 2011. 10

[3] Simon Baker and Shree K Nayar. A theory of single-viewpoint catadioptric image formation. *International Journal of Computer Vision*, 35(2):175–196, 1999. 10

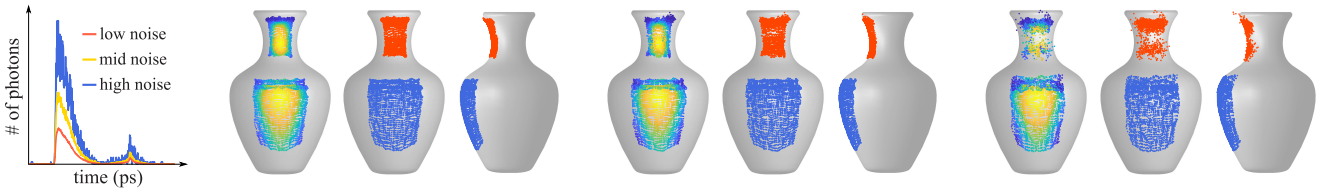

(a) simulated transients (b) reconstruction for low noise case (c) reconstruction for mid noise case (d) reconstruction for high noise case

Figure 2: **Reconstructions under different noise levels.** We show reconstructions from simulated transient measurements for a vase, rendered with three different noise levels. (a) Comparison of rendered transients for the three cases (representative sample). (b)-(d) For each case, we show reconstructed points colored by normal (left) and by branch of the Fermat pathlength function (middle and right).

[4] James W Bruce and Peter J Giblin. *Curves and Singularities: a geometrical introduction to singularity theory*. Cambridge university press, 1992. 7, 8

[5] James W Bruce, Peter J Giblin, and Christopher G Gibson. On caustics of plane curves. *The American Mathematical Monthly*, 88(9):651–667, 1981. 7, 8

[6] Quercus Hernandez, Diego Gutierrez, and Adrian Jarabo. A computational model of a single-photon avalanche diode sensor for transient imaging. *arXiv preprint arXiv:1703.02635*, 2017. 11

[7] Wenzel Jakob. Mitsuba renderer, 2010. http://www.mitsuba-renderer.org. 11

[8] Wenzel Jakob and Steve Marschner. Manifold exploration: A markov chain monte carlo technique for rendering scenes with difficult specular transport. *ACM Transactions on Graphics*, 2012. 10

[9] Michael Kazhdan and Hugues Hoppe. Screened poisson surface reconstruction. *ACM Transactions on Graphics (ToG)*, 32(3):29, 2013. 11

[10] Daniel Mayost. *Applications of the signed distance function to surface geometry*. PhD thesis, 2014. 9

[11] Michael Spivak. *Calculus on manifolds: a modern approach to classical theorems of advanced calculus*. CRC Press, 2018. 10

[12] Bruce Walter, Shuang Zhao, Nicolas Holzschuch, and Kavita Bala. Single scattering in refractive media with triangle mesh boundaries. In *ACM Transactions on Graphics (TOG)*, volume 28, page 92. ACM, 2009. 10

[13] Andrew Zisserman, Peter J Giblin, and Andrew Blake. The information available to a moving observer from specularities. *Image and vision computing*, 7(1):38–42, 1989. 9